

pubs.acs.org/crystal Article

Stabilizing Cationic Perylene Dimers through Pancake Bonding and Equal Charge Share

Megan E. McCormack, Rameswar Bhattacharjee, Henry Jervis, Zheng Wei, Miklos Kertesz,* and Marina A. Petrukhina*



Cite This: *Cryst. Growth Des.* 2023, 23, 7496–7503



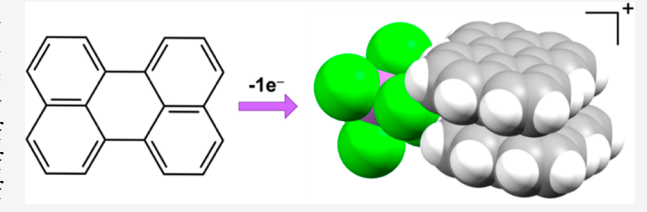
ACCESS I

III Metrics & More

Article Recommendations

Supporting Information

ABSTRACT: A cationic perylene salt was synthesized by chemical oxidation through treatment of perylene with triethyloxonium hexachloroantimonate in dichloromethane and characterized by single crystal X-ray diffraction as $[(C_{20}H_{12})_2]^{\bullet+}(SbCl_6)^-$. EPR spectrometry confirmed the formation of an organic radical with a g-factor of 2.0024. X-ray diffraction analysis revealed a 1D column stacking of perylene molecules with alternating interplanar distances of 3.255(2)-3.340(2) Å and 3.409(2)-3.466(3) Å, indicative of the



dimer formation within infinite π -stacks. Within a dimer, a large π -surface overlap and a slight loss of planarity for perylene were also observed. As these structural characteristics are consistent with pancake bonding for a perylene dimer, further insights into bonding were sought with the help of density functional theory. The calculations revealed that the pancake interaction contributes significantly to the stabilization of the stacked perylene dimer, providing approximately 8.0-10.0~kcal/mol per pair. Further stabilization is achieved by an even distribution of the positive charge in the monocationic dimer. A direct comparison with the close analogue revealed the critical role of the solid-state packing effects in achieving a higher degree of overlap between the perylene monomers in the title product.

INTRODUCTION

Since the discovery of graphene, ¹ the study of planar polycyclic aromatic hydrocarbons (PAHs) has come into greater focus due to their interesting physical and chemical properties. ² In particular, PAHs have been utilized as semiconductor materials in solar cells, ³ light-emitting diodes, ⁴ and organic field-effect transistors. ⁵ Additionally, the partial oxidation of PAHs has been shown to enable tunable conductivity and magnetism. ⁶ Upon oxidation and crystallization of small planar polyarenes, the formation of extended π -stacks of the delocalized radical cations with short interplanar distances has been observed, with these structural characteristics responsible for interesting conducting and magnetic properties. ⁷

Furthermore, pancake bonding interactions can be formed upon one-electron oxidation of PAHs. 8,9 The pancake bonding was first observed in the 1960s, 10 where highly overlapping π -stacks derived from an energy-lowering interaction of singly occupied molecular orbitals (SOMOs) form stable and energetically competitive dimers. The high overlap of SOMOs provides a two-electron multicenter (2e/mc) bonding interaction as the stabilizing component of these materials. 11,12 This orbital overlap gives rise to specific and consistent structural characteristics, which have been repeatedly observed with the help of single crystal X-ray diffraction and theoretical analysis. $^{13-16}$ These characteristics include intermolecular contacts shorter than van der Waals (vdW) radii, slight deviations of planarity, and highly overlapping configurations. 17

However, the controlled one-electron chemical oxidation of small planar polyarenes has been sparingly reported, and most methodologies remained focused on electrochemical oxidation. Perylene is a notable example of this phenomenon, where a number of cationic perylene products have been characterized crystallographically, yet the vast majority have been formed through anodic oxidation. As early as the 1970s, cationic perylene products have been isolated in a crystalline form, where electrochemical oxidation of perylene with various dithiolate tetrabutylammonium salts provided products with the $(C_{20}H_{12})_2[M(mnt)_2]$ composition (mnt = $S_2C_2(CN)_2$ M = Ni, Cu, Pd, ^{18,19} Au, Pt, ^{20,21} Fe, Co^{22,23}). In the 1980s and 1990s, electrochemical oxidation with tetrabutylammonium salts of PF₆⁻, AsF₆⁻, and ClO₄⁻ has been explored to afford perylene cation products with compositions of $(C_{20}H_{12})_2^+PF_6^-$, $(C_{20}H_{12})_2^+AsF_6^-$, $(C_{20}H_{12})_3^+ClO_4^-$, and $(C_{20}H_{12})_6^+ClO_4^-$. In 2001, electrochemical oxidation of perylene with tetrabutylammonium salts of Lindquist polyoxoanions afforded isostructural crystals of the compositions (C₂₀H₁₂)₅[Mo₆O₁₉], (C₂₀H₁₂)₅[W₆O₁₉], and

Received: July 31, 2023
Revised: September 7, 2023
Published: September 21, 2023





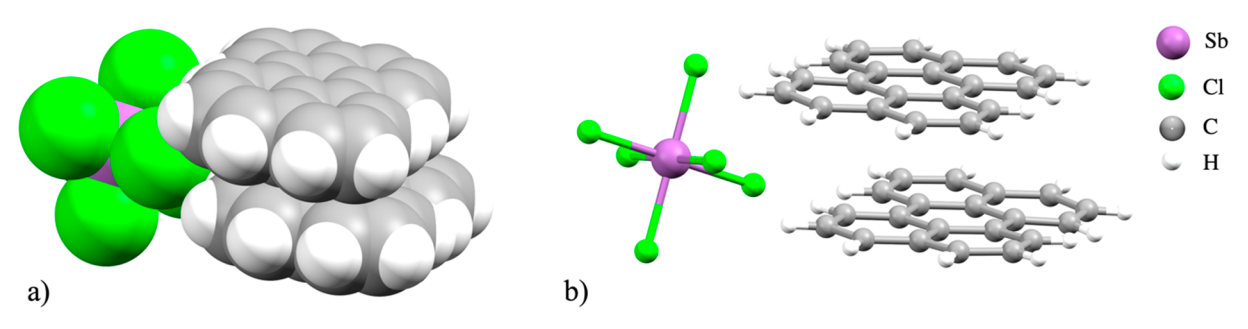


Figure 1. Crystal structure of $[(C_{20}H_{12})_2]^{\bullet+}(SbCl_6)^-$, a) space-filling model and b) ball-and-stick model.

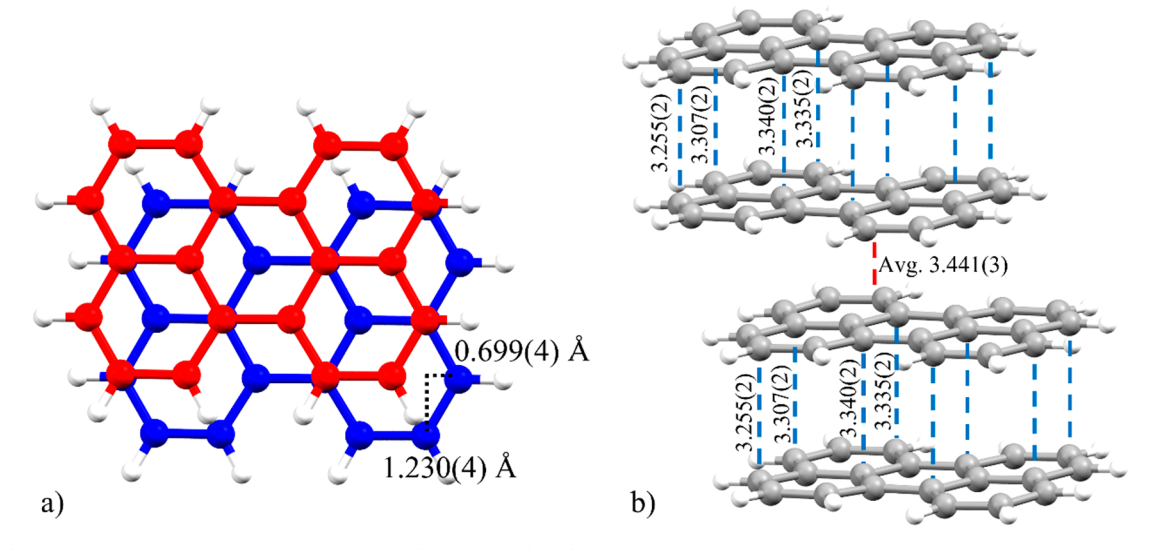


Figure 2. a) Atom-over-atom configuration of $[(C_{20}H_{12})_2]^{\bullet+}(SbCl_6)^-$. b) Interplanar contacts within perylene π -stacked columns.

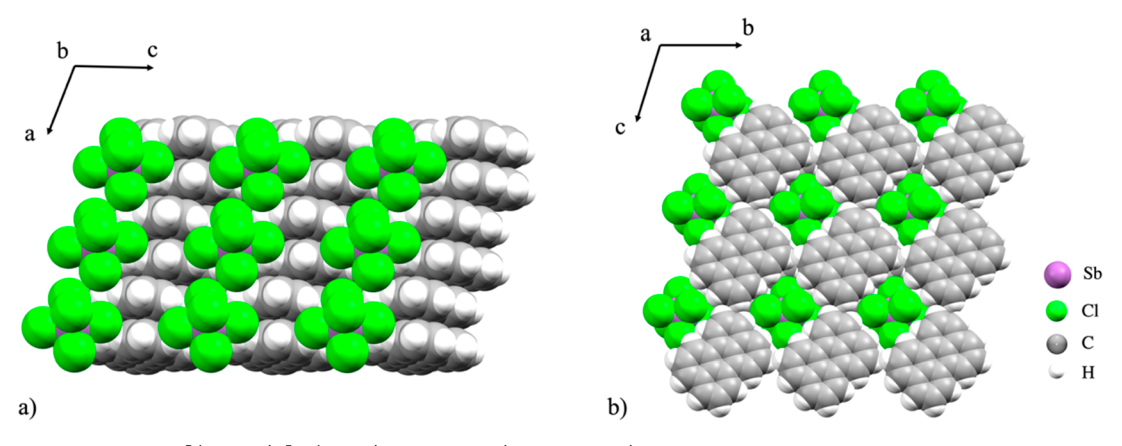


Figure 3. Solid-state packing of $[(C_{20}H_{12})_2]^{\bullet+}(SbCl_6)^-$ down the a) *b*-axis and b) *a*-axis, space-filling model.

 $(C_{20}H_{12})_5[VW_5O_{19}]$. Then in 2004, electrochemical oxidation of perylene with tetraalkylammonium salts of Keggin-type polyoxoanions yielded crystals of $(C_{20}H_{12})_6[PMo_{12}O_{40}]$. CH_2Cl_2 , $(C_{20}H_{12})_6[PMo_{12}O_{40}] \cdot CH_3CN$, and $(C_{20}H_{12})_9(NBu_4)_4[SiW_{12}O_{40}]_2$. These various cationic perylene products showed persistent structural characteristics, where continuous π -stacks are formed with interplanar contacts below the vdW radii. However, so far, no theoretical evaluation of bonding and electronics on any of these cationic perylene-based salts has been carried out. The fact that there is only one unpaired electron in the putative dimer indicates a formal intermolecular pancake bond order of 1/2. For this reason, a theoretical analysis should be useful in identifying the strength

and nature of the electron-sharing pancake bond in these dimers. 30,31

To the best of our knowledge, only one cationic perylene product has been formed exclusively through chemical oxidation, namely $[(C_{20}H_{12})_2]^{\bullet+}(C_{32}H_{12}BF_{24})^{-.32}$ Quantum mechanical calculations to determine reorganization energies and electronic coupling elements revealed high electron mobility along π -bonded stacks. Herein, we set to investigate the chemical oxidation of perylene with the one-electron oxidant triethlyoxonium hexachloroantimonate, $[Et_3O^+][SbCl_6^-]$. The resulting cationic radical perylene salt, $[(C_{20}H_{12})_2]^{\bullet+}(SbCl_6)^-$, has been isolated and characterized with single-crystal X-ray diffraction, EPR, and UV—vis spectroscopic methods. Further

Crystal Growth & Design pubs.acs.org/crystal Article

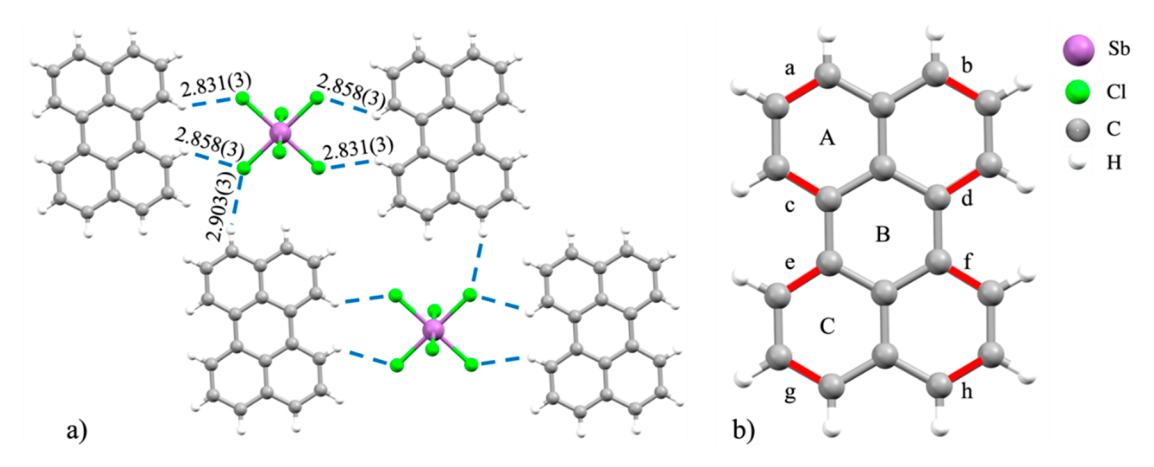


Figure 4. a) Hydrogen bonding contacts between perylene and SbCl₆⁻. b) Selected carbon-carbon bonds along with labeled rings.

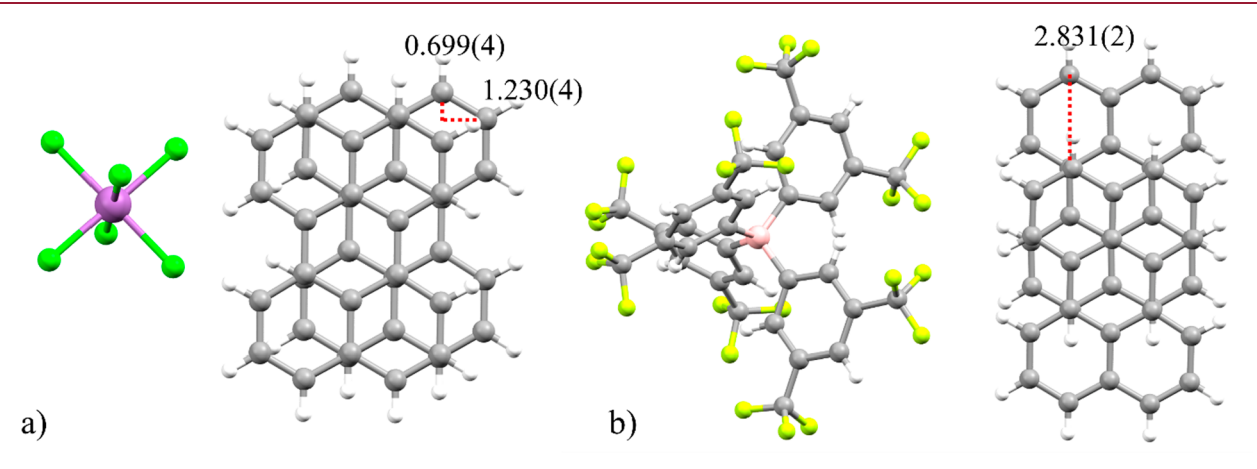


Figure 5. Surface overlap in a) $[(C_{20}H_{12})_2]^{\bullet+}(SbCl_6)^-$ and b) $[(C_{20}H_{12})_2]^{\bullet+}(C_{32}H_{12}BF_{24})^{-32}$

insights into bonding and electronic structure have been obtained with the help of computational methods.

RESULTS AND DISCUSSION

Preparation, Characterization, and Crystallographic Study of [$(C_{20}H_{12})_2$]*+ $(SbCl_6)^-$. Mixing perylene and [Et_3O^+]-[$SbCl_6^-$] in a 1:1.5 ratio in anhydrous DCM at room temperature afforded a green-brown solution within 2 min. Single crystals suitable for X-ray diffraction analysis were grown through layering the DCM solution with toluene and keeping the system at 5 °C. After 5 days, slow diffusion of toluene produced thin, deep blue needles in ca. 46% yield. The X-ray diffraction analysis confirmed the formation of the product with a composition of $[(C_{20}H_{12})_2]^{\bullet+}(SbCl_6)^-$ (Figure 1) and without any solvent incorporation. The crystals conform to the triclinic P-1 space group (Z=1) with a volume of 810.40(19) ų.

Based on the X-ray diffraction data, the formula unit contains two crystallographically equivalent perylene molecules per $SbCl_6^-$ anion. In the crystal structure, perylene molecules form 1D columns with alternating interplanar distances of 3.255(2)-3.340(2) and 3.409(2)-3.466(3) Å, thus showing the formation of the cationic perylene dimers $[(C_{20}H_{12})_2]^{\bullet+}$ within infinite π -stacks. Within the dimer, the two perylene molecules exhibit high surface overlap (Figure 2). In the solid-state, 1D perylene stacks are separated by the $SbCl_6^-$ anions, displaying alternating cationic and anionic columns (Figure 3).

Each perylene within the dimer has identical H···Cl hydrogen bonding interactions with the neighboring SbCl₆⁻ anions

(Figure 4a). These hydrogen bonding contacts range from 2.831(3) to 2.903(3) Å and contribute to the stability of the crystal structure. An observable carbon—carbon bond length elongation (average 0.015 Å) is observed at bonds a—h (Figure 4b), which range from 1.380(2) to 1.406(3) Å, while the corresponding aromatic C—C bonds of the neat perylene³³ range from 1.357(4) to 1.380(4) Å due to a reduction of the respective π -bond orders arising from the +1/2 charge on each perylene.

A further look into the perylene dimers shows a deviation from planarity in comparison with the uncharged parent. For the neutral perylene, a minor deviation from planarity of 0.87° is observed between rings A and B and 0.84° between rings A and C. The dimeric $[(C_{20}H_{12})_2]^{\bullet+}$ unit shows a more notable deviation from planarity of 2.05° and 2.58° between the respective rings. These rather similar changes in planarity and C–C bond elongation may indicate an even charge distribution within the perylene dimers. This has been confirmed by molecular orbital computations, as discussed below.

Notably, the previously reported $[(C_{20}H_{12})_2]^{\bullet+}$ $(C_{32}H_{12}BF_{24})^-$ salt shows structural similarity with the product reported in this work, $[(C_{20}H_{12})_2]^{\bullet+}(SbCl_6)^-$, namely a distinct dimer formation in continuous π -stacks with a good π -surface overlap (Figure 5).³²

The UV—vis absorption spectroscopy measurements were carried out by incremental addition of [Et₃O⁺][SbCl₆⁻] to a perylene solution in DCM, revealing a quick color change from pale yellow-orange (390, 412, and 438 nm) to a bright purple

(544 nm) (Figure S1). Notably, the UV—vis spectra are similar to that reported for $[(C_{20}H_{12})_2]^{\bullet+}(C_{32}H_{12}BF_{24})^{-.32}$ The crystals of the title product showed good stability in air based on the solid-state reflectance UV—vis spectra (Figure S2). To confirm radical formation, EPR spectra were collected on a crystalline sample of $[(C_{20}H_{12})_2]^{\bullet+}(SbCl_6)^-$. A high intensity singlet was observed with a g-factor of 2.0024, consistent with the formation of an organic radical (Figure 6).

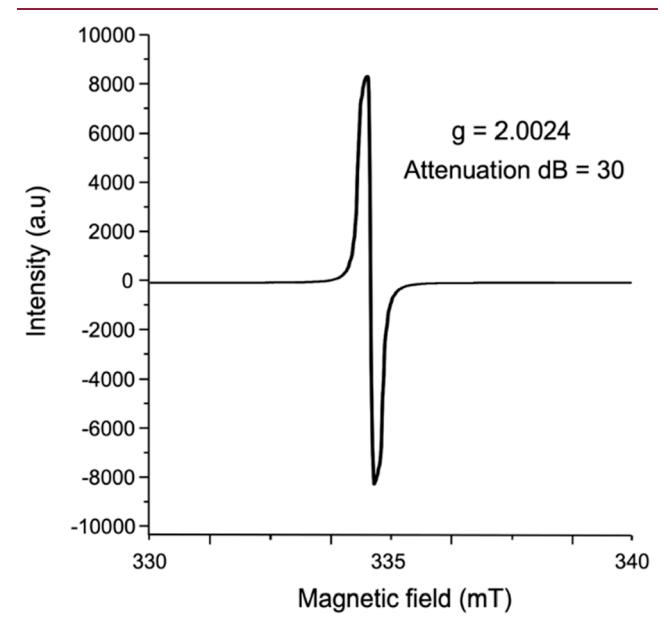


Figure 6. EPR spectrum of $[(C_{20}H_{12})_2]^{\bullet+}(SbCl_6)^-$ collected at 29.2 °C on a LINEV ADANI Spinscan X Electron Paramagnetic Resonance Spectrometer.

Due to the apparent product stability in air, conductivity studies on a pressed pellet of $[(C_{20}H_{12})_2]^{\bullet+}(SbCl_6)^-$ were performed. Repeated measurements revealed a conductivity of 0.0055 S/cm at 298 K, which is close to the reported value of 0.004 S/cm (295 K) obtained for the perylene cationic salt, $[(C_{20}H_{12})_2]^{\bullet+}(SbF_6)^{-}$. However, no single crystal structure of the above salt was reported by Wegner et al., and the product composition was later assigned based on X-ray powder diffraction, optical absorption spectroscopy, and EPR spectros-

copy.³⁵ For the previously reported $[(C_{20}H_{12})_2]^{\bullet+}$ $(C_{32}H_{12}BF_{24})^-$, conductivity measurements were not performed. Instead, a combination of Near-Infrared (NIR) spectroscopy and coupling elements allowed an approximation of electron mobility, where intensities in the NIR and IR ranges fitted the conditions necessary for metallic conduction and the high values of coupling elements suggested high hole mobility through perylene π -stacks.³²

Computational Investigation. In the computational study, we utilized two different models of perylene dimers in order to represent the $[(C_{20}H_{12})_2]^{\bullet+}$ unit: one based on the dimer extracted from the title crystal structure, and another based on the previously reported X-ray structure³² of $[(C_{20}H_{12})_2]^{\bullet+}(C_{32}H_{12}BF_{24})^-$. Figure 5 illustrates the distinct relative orientations of the two adjacent perylenes forming monocationic dimers in these two structures. Hence, we referred to the dimer obtained from $[(C_{20}H_{12})_2]^{\bullet+}(SbCl_6)^-$ as $[(C_{20}H_{12})_2]_A^{\bullet+}$ and the dimer obtained from $[(C_{20}H_{12})_2]^{\bullet+}(C_{32}H_{12}BF_{24})^-$ as $[(C_{20}H_{12})_2]_B^{\bullet+}$ for the sake of convenience in our computations and discussions.

In Figure 7, we present the optimized structures of the $[(C_{20}H_{12})_2]^{\bullet+}$ dimers, showcasing the shortest intermolecular C-C contact distances. It was reassuring to see that both optimized dimeric monocation perylene structures retained the intermolecular overlap pattern observed in their respective experimental structures. Furthermore, there is variation in the number of short contacts between the perylene molecules within the two dimers. We identified eight short contacts in $[(C_{20}H_{12})_2]_A^{\bullet+}$ ranging from 3.27 to 3.36 Å. Conversely, the previously reported dimer $[(C_{20}H_{12})_2]_B^{\bullet+}$, exhibits seven short C-C contacts. The increased number of short contacts in the former dimer plays a crucial role in achieving a higher degree of overlap between the perylene monomers, consistent with our experimental observations (Figure S4). Notably, the C-C distances in the latter dimer are comparatively shorter, ranging from 3.22 to 3.27 Å.

Understanding the interaction between two perylene units in the dimer is crucial to comprehending the stability of this conformation. To gain insight into this aspect, we performed calculations to determine the interaction energy of perylene in both dimers. Interestingly, despite the distinct conformations and varying number of short contacts in $[(C_{20}H_{12})_2]_A^{\bullet+}$ and $[(C_{20}H_{12})_2]_B^{\bullet+}$, their interaction energies are quite comparable.

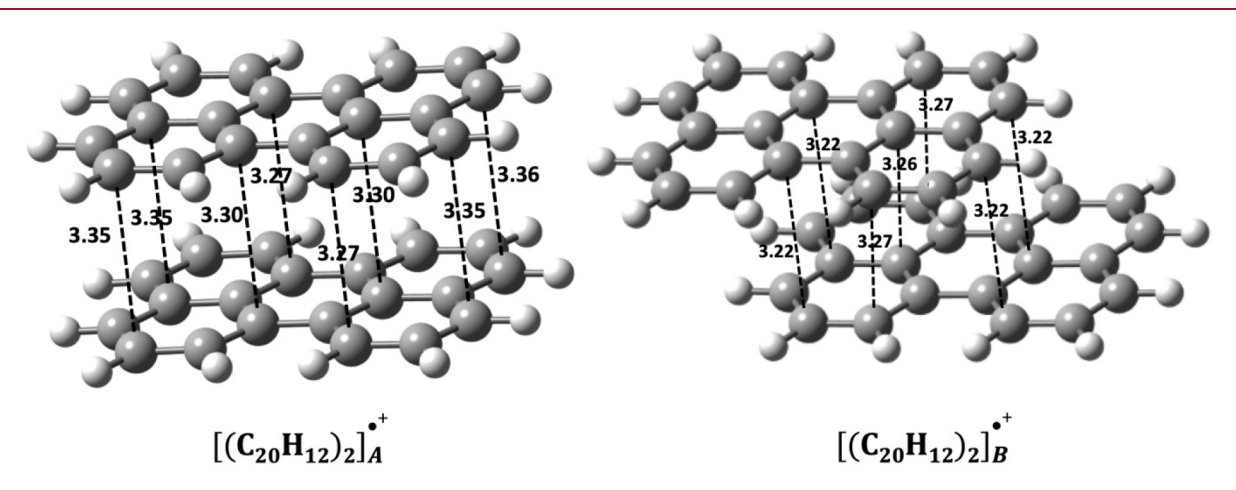


Figure 7. Optimized geometries of the $[(C_{20}H_{12})_2]^{\bullet+}$ dimer derived from the present study and a previously reported crystal structure.³² The intermolecular C-C short distances are expressed in angstroms (Å).

Crystal Growth & Design pubs.acs.org/crystal Article

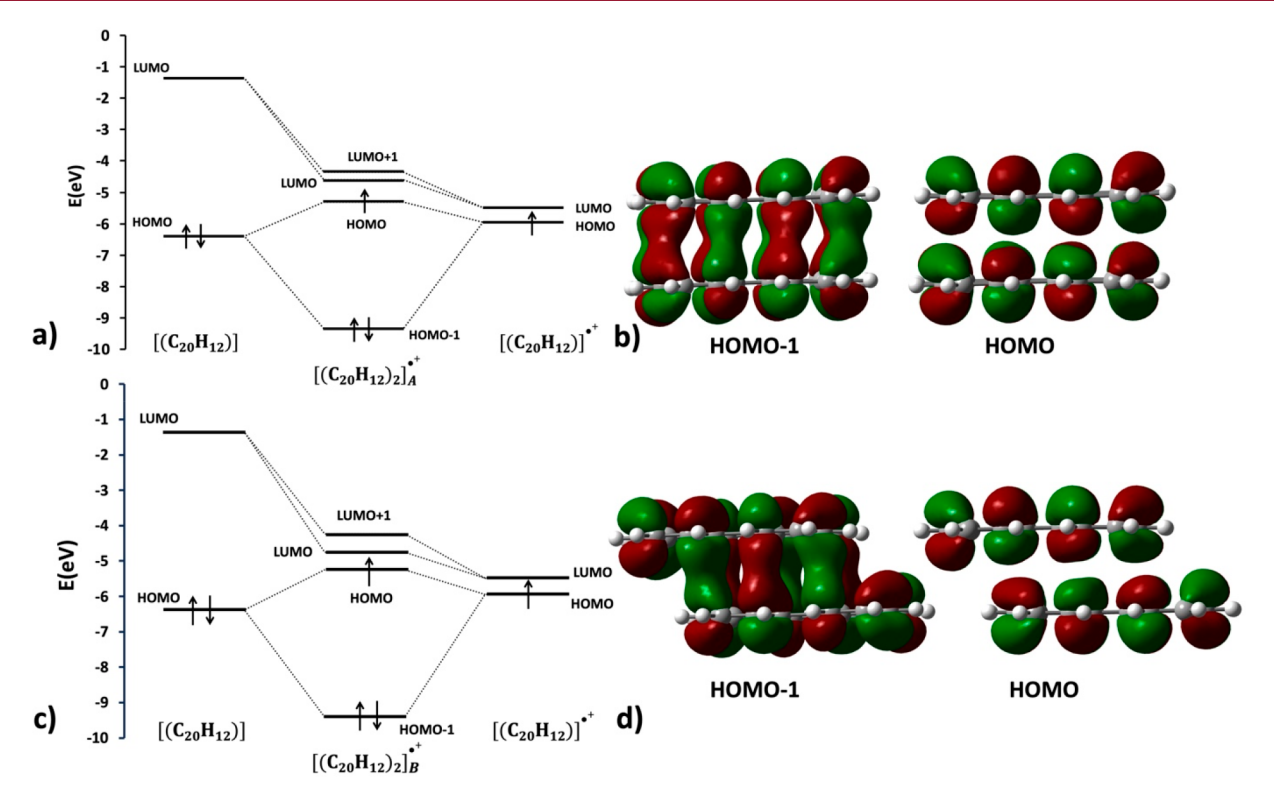


Figure 8. a) Molecular orbital diagram of $[(C_{20}H_{12})_2]_A^{\bullet+}$, obtained by combining a neutral perylene unit with a positively charged perylene unit. b) HOMO-1 and HOMO orbitals of $[(C_{20}H_{12})_2]_A^{\bullet+}$. c) Molecular orbital diagram of $[(C_{20}H_{12})_2]_B^{\bullet+}$. d) HOMO-1 and HOMO orbitals of $[(C_{20}H_{12})_2]_B^{\bullet+}$.

The interaction energy for $[(C_{20}H_{12})_2]_A^{\bullet+}$ is -20.3 kcal/mol, while for $[(C_{20}H_{12})_2]_B^{\bullet+}$ it is -21.1 kcal/mol. It is worth noting that these interaction energies are relatively high, warranting further investigation.

In Figure 8a, we can see the molecular orbital diagram of $[(C_{20}H_{12})_2]_A^{\bullet+}$, which is formed by the interaction of a neutral and positively charged perylene unit. The diagram demonstrates that the highest occupied molecular orbitals (HOMO) of $[(C_{20}H_{12})]^{\bullet+}$ and $[(C_{20}H_{12})_2]$ combine to create the HOMO and HOMO-1 of the dimer. Within the dimer, the HOMO-1 is occupied by two electrons, while the HOMO is occupied by a single electron. Both orbitals are presented in Figure 8b, revealing that the HOMO-1 is a bonding orbital (BO), exhibiting clear in-phase intermolecular carbon—carbon orbital overlap. This type of intermolecular overlap is known as a pancake bond. On the other hand, the HOMO is an antibonding orbital (ABO) of HOMO-1, and it contains a single electron.

The occupation of the HOMO-1 by two electrons and HOMO by one electron, respectively, results in a pancake bond order (PBO) of 1/2, calculated as PBO = (Occupation in BO – Occupation in ABO)/2. (Note that other cases of partial pancake bond order are also known, see ref 36). Therefore, it can be argued that the HOMO-1 primarily contributes to the pancake interaction in $[(C_{20}H_{12})_2]_A^{\bullet+}$, which is not a common observation in the pancake bonding literature, where the HOMO is typically identified as the orbital primarily responsible for stabilizing the intermolecular interaction. The stronger binding energy between the perylene units in $[(C_{20}H_{12})_2]_A^{\bullet+}$ can also be attributed to the efficient intermolecular orbital overlap present in the system. Similar findings are observed for the other dimer, $[(C_{20}H_{12})_2]_B^{\bullet+}$, and the corresponding orbital diagram with the orbital plots can be found in Figure 8 (c and d).

In addition to examining the orbital properties, we also analyzed the charge distributions within the perylene dimers. We calculated the natural bond orbital (NBO) charges for both $[(C_{20}H_{12})_2]_A^{\bullet+}$ and $[(C_{20}H_{12})_2]_B^{\bullet+}$, and found that the +1 charge of the dimers is evenly distributed in each monomer with a charge of +0.5. This equal charge distribution is further supported by the spin density plots of both dimers, where the spin is observed to be delocalized across both monomers in the dimer (Figure 9). To further validate the equal charge

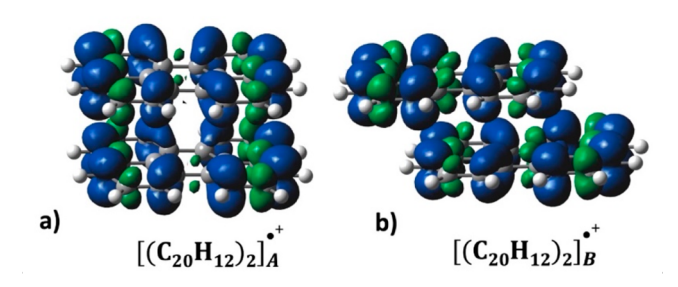
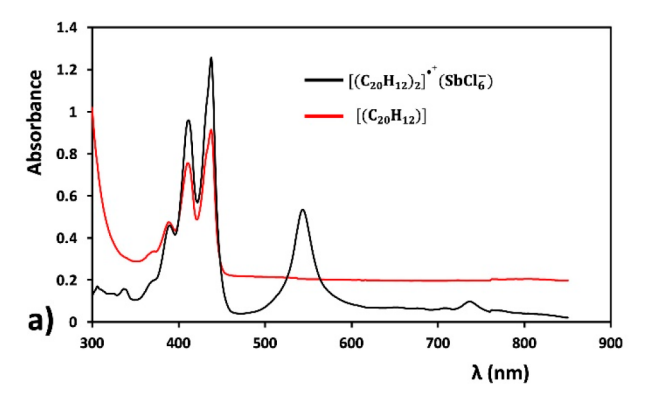


Figure 9. Spin density plot of a) $[(C_{20}H_{12})_2]_A^{\bullet+}$ and b) $[(C_{20}H_{12})_2]_B^{\bullet+}$, displaying the spatial distribution of spin density within the molecule. The spin densities are visualized using a density isovalue of 0.0008.

distribution, we performed periodic DFT calculations on the crystal structure of $[(C_{20}H_{12})_2]^{\bullet+}(SbCl_6)^-$ and conducted a Bader charge analysis. The Bader charge analysis of the crystal produced a total charge value for the perylene dimer of +0.9e, with each monomer carrying a charge of +0.45e, further confirming the equal distribution of charges. Overall, these findings demonstrate that the +1 charge in the perylene dimers, as observed in $[(C_{20}H_{12})_2]_A^{\bullet+}$ and $[(C_{20}H_{12})_2]_B^{\bullet+}$, is equally shared between the two monomers, and this equal charge



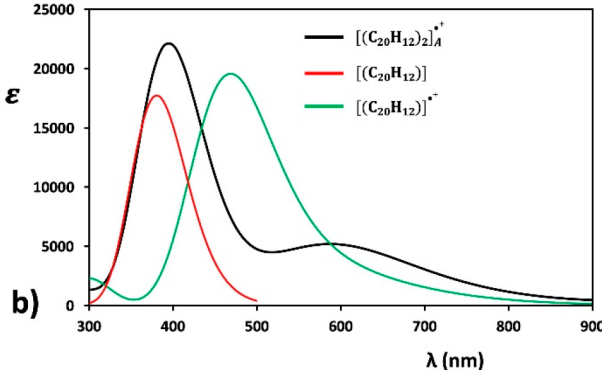


Figure 10. a) UV—vis absorption spectra of crystals of $[(C_{20}H_{12})_2]^{\bullet+}(SbCl_6)^-$ dissolved in DCM and neat perylene dissolved in DCM. b) Computed UV—vis spectra of $[(C_{20}H_{12})_2]_A^{\bullet+}$ (black line). The green and red lines are the computed spectra for the neutral and cationic monomer, respectively. Gaussian broadening of 0.333 eV was used.

distribution is consistent across different methods, including NBO charges, spin density plots, and Bader charge analysis of the crystal structure.

To gain further insight into the optical properties of the perylene dimer, we conducted TD-DFT calculations to determine the UV–visible spectra of the $[(C_{20}H_{12})_2]_A^{\bullet+}$ dimer, as well as the individual monomers in their neutral and positively charged states. The obtained results are illustrated in Figure 10 together with the experimental spectra, which show a series of vibrational subbands.

In the computed spectrum of the dimer, two distinct peaks were observed. The first peak, located at approximately 400 nm, displayed a high intensity. Interestingly, a similar peak was also observed in the UV—visible spectra of the isolated neutral and positively charged perylene monomers. Hence, this peak at 400 nm can be attributed to the presence of the perylene molecule, suggesting that it retains its characteristic optical behavior, even in the dimeric form. However, the second peak observed in the dimer's spectrum, positioned around 580 nm, exhibited a broader shape and lower intensity compared to the peak at 400 nm. This peak at 580 nm was not observed in the UV—visible spectra of the neutral or positively charged perylene monomers. Consequently, this peak at ~580 nm is a distinctive characteristic of the pancake bonded dimer, which is in excellent agreement with the solution experiment.

CONCLUSION

Through the chemical oxidation of perylene with $[Et_3O^+]-[SbCl_6^-]$ and subsequent crystallization, single crystals of the $[(C_{20}H_{12})_2]^{\bullet+}(SbCl_6)^-$ composition were isolated and characterized crystallographically and spectroscopically. The EPR measurements further supported the formation of an organic-based radical (g=2.0024). Structural analysis revealed 1D columnar packing of perylene molecules with alternating shorter and longer interplanar distances of 3.255(2)-3.340(2) Å and 3.409(2)-3.466(3) Å, thus showing distinct dimer pair formation within π -stacks. As each dimer shows a large intradimer π -surface overlap, this prompted a thorough theoretical investigation of the bonding and electronic structures of the title product.

Density functional theory (DFT)-based calculations were employed to gain insights into the structure, electronic properties, and nature of perylene—perylene interactions within the dimer. The calculations revealed that the perylene molecules in the dimer are interconnected not only through van der Waals

interactions but also through a distinctive intermolecular electron sharing known as a pancake bonding interaction. This pancake interaction contributes significantly to the stabilization of the stacked dimer, providing approximately 8.0–10.0 kcal/mol per pair. The computed molecular diagram and orbital plots highlight that the HOMO-1 orbital plays a crucial role in facilitating the pancake interaction within the dimer. Moreover, analysis of different charge models and spin density confirms the equal distribution of the total +1 charge between the monomers in the perylene dimer in the crystal.

ASSOCIATED CONTENT

Supporting Information

The Supporting Information is available free of charge at https://pubs.acs.org/doi/10.1021/acs.cgd.3c00912.

Experimental and computational details, UV—vis spectra, EPR spectroscopy and conductivity sample preparation details, single crystal X-ray diffraction data (PDF)

Accession Codes

CCDC 2282180 contains the supplementary crystallographic data for this paper. These data can be obtained free of charge via www.ccdc.cam.ac.uk/data_request/cif, or by emailing data_request@ccdc.cam.ac.uk, or by contacting The Cambridge Crystallographic Data Centre, 12 Union Road, Cambridge CB2 1EZ, UK; fax: +44 1223 336033.

AUTHOR INFORMATION

Corresponding Authors

Miklos Kertesz — Chemistry Department and Institute of Soft Matter, Georgetown University, Washington, D.C. 20057-1227, United States; orcid.org/0000-0002-7930-3260; Email: kertesz@georgetown.edu

Marina A. Petrukhina — Department of Chemistry, University at Albany, State University of New York, Albany, New York 12222, United States; Ocid.org/0000-0003-0221-7900; Email: mpetrukhina@albany.edu

Authors

Megan E. McCormack — Department of Chemistry, University at Albany, State University of New York, Albany, New York 12222, United States

Rameswar Bhattacharjee — Chemistry Department and Institute of Soft Matter, Georgetown University, Washington, D.C. 20057-1227, United States; orcid.org/0000-0002-6631-5991

- **Henry Jervis** Chemistry Department and Institute of Soft Matter, Georgetown University, Washington, D.C. 20057-1227, United States
- Zheng Wei Department of Chemistry, University at Albany, State University of New York, Albany, New York 12222, United States

Complete contact information is available at: https://pubs.acs.org/10.1021/acs.cgd.3c00912

Notes

The authors declare no competing financial interest.

ACKNOWLEDGMENTS

Financial support of this work from the U.S. National Science Foundation, CHE-2003411 (M.A.P) and CHE-2107820 (M.K.), is gratefully acknowledged. Additionally, NSF's ChemMatCARS, Sector 15 at the Advanced Photon Source (APS), Argonne National Laboratory (ANL) is supported by the Divisions of Chemistry (CHE) and Materials Research (DMR), National Science Foundation, under grant number NSF/CHE-1834750. This research used resources of the Advanced Photon Source, a U.S. Department of Energy (DOE) Office of Science user facility operated for the DOE Office of Science by Argonne National Laboratory under Contract No. DE-AC02-06CH11357.

REFERENCES

- (1) Geim, A. K.; Novoselov, K. S. The Rise of Graphene. *Nat. Mater.* **2007**, *6*, 183–191.
- (2) Anthony, J. E. Functionalized Acenes and Heteroacenes for Organic Electronics. *Chem. Rev.* **2006**, *106*, 5028–5048.
- (3) Tremblay, N. J.; Gorodetsky, A. A.; Cox, M. P.; Schiros, T.; Kim, B.; Steiner, R.; Bullard, Z.; Sattler, A.; So, W.; Itoh, Y.; Toney, M. F.; Ogasawara, H.; Ramirez, A. P.; Kymissis, I.; Steigerwald, M. L.; Nuckolls, C. Photovoltaic Universal Joints: Ball-and-Socket Interfaces in Molecular Photovoltaic Cells. *ChemPhysChem* **2010**, *11*, 799–803.
- (4) Lee, K. H.; Park, J. K.; Seo, J. H.; Park, S. W.; Kim, Y. S.; Kim, Y. K.; Yoon, S. S. Efficient Deep-Blue and White Organic Light-Emitting Diodes Based on Triphenylsilane-Substituted Anthracene Derivatives. *J. Mater. Chem.* **2011**, *21*, 13640–13648.
- (5) Zhan, X.; Zhang, J.; Tang, S.; Lin, Y.; Zhao, M.; Yang, J.; Zhang, H.-L.; Peng, Q.; Yu, G.; Li, Z. Pyrene Fused Perylene Diimides: Synthesis, Characterization and Applications in Organic Field-Effect Transistors and Optical Limiting with High Performance. *Chem. Commun.* **2015**, *51*, 7156–7159.
- (6) Morita, Y.; Suzuki, S.; Fukui, K.; Nakazawa, S.; Kitagawa, H.; Kishida, H.; Okamoto, H.; Naito, A.; Sekine, A.; Ohashi, Y.; Shiro, M.; Sasaki, K.; Shiomi, D.; Sato, K.; Takui, T.; Nakasuji, K. Thermochromism in an Organic Crystal Based on the Coexistence of σ and π -Dimers. *Nat. Mater.* **2008**, *7*, 48–51.
- (7) Kröhnke, C.; Enkelmann, V.; Wegner, G. Radical Cations Salts of Simple Arenes A New Family of "Organic Metals. *Angew. Chem., Int. Ed. Engl.* **1980**, *19*, 912–913.
- (8) Kosower, E. M.; Cotter, J. L. Free Radicals II. The Reduction of 1-methyl-4-cyanopryidinum Ion to Methylviologen Cation Radical. *J. Am. Chem. Soc.* **1964**, *86*, 5524–5527.
- (9) Bockman, T. M.; Kochi, J. K. Isolations and Oxidation-Reduction of Methylviologen Cation Radicals. Novel Disproportionation in Charge-Transfer Salts by X-ray Crystallography. *J. Org. Chem.* **1990**, *55*, 4127–4135.
- (10) Mulliken, R. S.; Person, W. B. Molecular Complexes; Wiley: Chichester; 1969, Chapter 16, p 259.
- (11) Novoa, J. J.; Lafuente, P.; Del Sesto, R. E.; Miller, J. S. Exceptionally Long (\geq 2.9 Å) C–C Bonds between [TCNE]⁻ Ions: Two-Electron, Four-Center π^* - π^* C–C Bonding in π -[TCNE]₂². *Angew. Chem., Int. Ed.* **2001**, 40, 2540–2545.

- (12) Cui, Z.; Lischka, H.; Beneberu, H. Z.; Kertesz, M. Rotational Barrier in Phenalenyl Neutral Radical Dimer: Separating Pancake and van der Waal Interactions. *J. Am. Chem. Soc.* **2014**, *136*, 5539–5542.
- (13) Goto, K.; Kubo, T.; Yamamoto, K.; Nakasuji, K.; Sato, K.; Shiomi, D.; Takui, T.; Kubota, M.; Kobayashi, T.; Yakusi, K.; Ouyang, J. A Stable Neutral Hydrocarbon Radical: Synthesis, Crystal Structure, and the Physical Properties of 2,5,8-tri-tert-butyl-phenalenyl. *J. Am. Chem. Soc.* **1999**, *121*, 1619–1620.
- (14) Suzuki, S.; Morita, Y.; Fukui, K.; Sato, K.; Shiomi, D.; Takui, T.; Nakasuji, K. Aromaticity on the Pancake Bonded Dimer of Neutral Phenalenyl Radical as Studies by MS and NMR Spectroscopy and NICS Analysis. *J. Am. Chem. Soc.* **2006**, *128*, 2530–2531.
- (15) Mandal, S. K.; Samanta, S.; Itkis, M. E.; Jensen, D. W.; Reed, R. W.; Oakley, R. T.; Tham, F. S.; Donnadieu, B.; Haddon, R. C. Resonating Valence Bond Ground State in Oxygen-Functionalized Phenalenyl-Based Neutral Radical Molecular Conductors. *J. Am. Chem. Soc.* 2006, 128, 1982–1994.
- (16) Huang, J.; Kertesz, M. Intermolecular Covalent π - π Bonding Interaction Indicated by Bond Distances, Energy Bands, and Magnetism in Biphenalenyl Biradicaloid Molecular Crystal. *J. Am. Chem. Soc.* **2007**, 129, 1634–1643.
- (17) Kertesz, M. Pancake Bonding: An Unusual Pi-Stacking Interaction. *Chem.—Eur. J.* **2019**, 25, 400–416. Cui, Z.-h.; Gupta, A.; Lischka, H.; Kertesz, M. Concave or convex π -dimers: the role of the pancake bond in substituted phenalenyl radical dimers. *Phys. Chem. Chem. Phys.* **2015**, 17, 23963–23969.
- (18) Alcácer, L.; Maki, A. H. Electrically Conducting Metal Dithiolate-Perylene Complexes. *J. Phys. Chem.* **1974**, 78 (3), 215–217.
- (19) Alcácer, L.; Maki, A. H. Magnetic Properties of Some Electrically Conducting Perylene-Metal Dithiolate Complexes. *J. Phys. Chem.* **1976**, 80 (17), 1912–1916.
- (20) Alcácer, L.; Novais, H.; Pedroso, F.; Flandrois, S.; Coulon, C.; Chasseau, D.; Gaultier, J. Synthesis, Structure and Preliminary Results on Electrical and Magnetic Properties of (Perylene)₂[Pt(mnt)₂]. *Solid State Commun.* **1980**, 35 (12), 945–949.
- (21) Domingos, A.; Henriques, R. T.; Gama, V.; Almeida, M.; Lopes-Vieira, A.; Alcacer, L. Crystalline Structure/Transport Properties Relationship in the $(Perlyene)_2M(mnt)_2$ Family (M = Au, Pd, Pt, Ni). *Synth. Met.* **1988**, 27, 411–416.
- (22) Matos, M.; Bonfait, G.; Santos, I. C.; Afonso, M. L.; Henriques, R. T.; Almeida, M. The Solid Solutions (Per)₂[Pt_xAu_(x-1)(mnt)₂]; Alloying Para- and Diamagnetic Anions in Two-Chain Compounds. *Magnetochemistry* **2017**, *3* (2), 22–35.
- (23) Gama, V.; Henriques, R. T.; Bonfait, G.; Pereira, L. C.; Waerenborgh, J. C.; Santos, I. C.; Duarte, M. T.; Cabral, J. M. P.; Almeida, M. Low-Dimensional Molecular Metals (Per)₂[M(mnt)₂] (M = Fe and Co). *Inorg. Chem.* **1992**, *31* (12), 2598–2604.
- (24) Keller, H. J.; Nöthe, D.; Pritzkow, H.; Dehe, D.; Werner, M.; Harms, R. H.; Koch, P.; Schweitzer, D. Electrochemical Synthesis of New One-Dimensional Metals: Radical Salts of Perylene. *Chem. Scr.* **1981**, *71*, 101–102.
- (25) Kuhs, W. F.; Mattern, G.; Brutting, W.; Dragan, H.; Burggraf, M.; Pilawa, B.; Dormann, E. Electrocrystallization, Crystal Structure and Physical Properties of Hexaperylene Hexafluorophosphate, $(C_{20}H_{12})_6^+PF_6^-$. Acta Crystallogr. 1994, B50, 741–746.
- (26) Burggraf, M.; Dragan, H.; gruner-Bauer, P.; Helberg, H. W.; Kuhs, W. F.; Mattern, G.; Müller, D.; Wendl, W.; Wolter, A.; Dormann, E. Z. The Peierls Transition of Perylene Radical Cations Salts with 2:1 Stochiometry Containing Tetrahydrofuran. *Physik B* **1995**, *96*, 439–450.
- (27) Endres, H.; Keller, H. J.; Müller, B. Electrocrystallization and Structures of Perylene Radical Salts: Hexaperylene Perchlorate, $(C_{20}H_{12})_6^+\text{ClO}_4^-$, Triperylene Perchlorate, $(C_{20}H_{12})_3^+\text{ClO}_4^-$, and Diperylene Hexafluorophospate-Tetrahydrofuran (2/3), $(C_{20}H_{12})_2^+\text{PF}_6^-\cdot 2/3\text{THF}$. Acta Crystallogr. 1985, C41, 607–613.
- (28) Clemente-León, M.; Coronado, É.; Giménez-Saiz, C.; Gómez-Garcia, C. J.; Martínez-Ferrero, E.; Almeida, M.; Lopes, E. B. Organic/Inorganic Molecular Conductors Based Upon Perylene and Lindquist-Type Polyoxometalates. *J. Mater. Chem.* **2001**, *11*, 2176–2180.

- (29) Coronado, E.; Galán-Mascarós, J. R.; Giménez-Saiz, C.; Gómez-Garcia, C. J.; Martínez-Ferrero, E.; Almeida, E.; Lopes, E. B.; Capelli, S. C.; Llusar, R. M. New Conducting Radical Salts Based Upon Keggin-Type Polyoxometalates and Perylene. *J. Mater. Chem.* **2004**, *14*, 1867–1872.
- (30) Small, D.; Zaitsev, V.; Jung, Y. S.; Rosokha, S. V.; Head-Gordon, M.; Kochi, J. K. Intermolecular, pi-to-pi Bonding Between Stacked Aromatic Dyads. Experimental and Theoretical Binding Energies and Near-IR Optical Transitions for Phenalenyl Radical/Radical Versus Radical/Cation Dimerizations. J. Am. Chem. Soc. 2004, 126, 13850—13858.
- (31) Cui, Z.; Wang, M.; Lischka, H.; Kertesz, M. Unexpected Charge Effects Strengthen π -Stacking Pancake Bonding. *JACS Au* **2021**, 1, 1647–1655.
- (32) Rosokha, S. V.; Stern, C. L.; Ritzert, J. T. π-Bonded Molecular Wires: Self-Assembly of Mixed-Valence Cation-Radical Stacks Within the Nanochannels formed by Inert Tetrakis[3,5-bis(trifluoromethyl)-phenyl]borate Anions. *CrystEngComm.* **2013**, *15*, 10638–10647.
- (33) Zhang, P.; Zeng, J.; Zhuang, F.; Zhao, K.; Sun, Z.; Yao, Z.; Lu, Y.; Wang, X.; Wang, J.; Pei, J. Parent B₂N₂-Perylenes with Different BN Orientations. *Angew. Chem., Int. Ed.* **2021**, *60*, 23313–23319.
- (34) Dellinger, B.; Lomnicki, S.; Khachatryan, L.; Maskos, Z.; Hall, R. W.; Adounkpe, J.; McFerrin, C.; Truong, H. Formation and Stabilization of Persistent Free Radicals. *Proc. Combust Inst.* **2007**, *31*, 521–528.
- (35) Hamm, S.; Wachtel, H. Rectifying Organic Junctions of Molecular Assemblies Based on Perylene Ion Salts. *J. Chem. Phys.* **1995**, *103*, 10689–10695.
- (36) Molcanov, K.; Mou, Z.; Kertesz, M.; Kojic-Prodic, B.; Stalke, D.; Demeshko, S.; Santic, A.; Stilinovic, V. Pancake Bonding in π -Stacked Trimers in a Salt of Tetrachloroquinone Anion. *Chem.—Eur. J.* **2018**, 24, 8292–8297.